

Virtual Reality Robot-Assisted Welding Based on Human Intention Recognition

Qiyue Wang^{id}, Wenhua Jiao^{id}, Rui Yu, Michael T. Johnson^{id}, *Senior Member, IEEE*,
and YuMing Zhang^{id}, *Senior Member, IEEE*

Abstract—We propose an innovative approach to enhance welding operations by using a cyber-physical system (CPS) with layered architecture and enabling a robot to be effectively operated by its commanding human. This article focuses on the recognition of the commanding human's intention that should be executed by the robot. To this end, a virtual reality (VR) system based on the HTC Vive is used to create a remote virtual welding environment. Human hand movement speed data is collected and used to train a hidden Markov model (HMM) using the Baum-Welch algorithm. The Bayesian information criterion (BIC) is applied to determine the number of hidden states. The state occupancy probability distribution (the probability of each state at a given time) is estimated based on the human hand movement speed sequence using the forward algorithm. The human intention, defined as the intended movement in this article, is then estimated as the statistical expectation of the observable variables. Using the proposed human intention estimation algorithm, the intended movement recognized from the raw movement data is smoother, which is preferable in welding tasks. A 6-DoF industrial robot, UR-5 with a custom gas tungsten arc welding (GTAW) torch installed, works as the final performer of the welding jobs. The robot receives the intended movement data from the HMM and uses this to assist the human welding operators. Welding experiments have been conducted both with and without the proposed human intention recognition (IR) algorithm. The results show that the robot can help the operators complete welding tasks with better performance using the proposed IR system, supporting the effectiveness of the proposed VR robot-assisted welding system.

Note to Practitioners—Welding is not only labor-intensive but also requires real-time adaption to the process, which is challenging for robots/machines but relatively straightforward for humans. Using a human commanded robot to perform welding can liberate humans from laborious operations and hazardous environments. To this end, a virtual reality (VR) system is used to create a virtual welding environment for a human to view the process remotely and for a human to pass his/her resultant

adaptation to the robot through hand movements. However, hand movements do not always fully represent the intended adaptation of the commanding human, and the recognition of such human intention is fundamental in such a proposed method. This article established the mathematical framework for the recognition of the human intention and, thus, the foundation for effective assistance of robots to humans.

Index Terms—Cyber-physical systems (CPSs), hidden Markov models (HMMs), human intention recognition (IR), robot-assisted welding, virtual reality (VR).

I. INTRODUCTION

WELDING robots have been widely used in industry and account for over 50% of industrial robots in the United States and globally [1]. However, these robots are typically only effective for structured, large-volume welding tasks considering the cost, both in economics and time. In unstructured and small-volume manufacturing, human welders currently still play an important role. However, they are often exposed to hazardous agents, such as fume and radiation [2]. Moreover, we are facing a substantial shortage of welders, especially highly skilled ones, according to the American Welding Society (AWS) [3]. Assisting less skillful welders to accomplish welding tasks well has become an urgent problem in industrial manufacturing. Many other complex operations also face a similar problem: human physical limitations constrain performance and efficiency, but human judgments are critical for operation success. Developing robot-assisted systems is an effective solution to such a problem [4].

A few robot-assisted surgery systems have been developed for a variety of surgeries [5]–[9] and commercialized successfully [10], [11]. Surgeons operated robots through different interfaces, such as a keyboard, a joystick, and a haptic controller [12]–[15]. Skills in operating through these interfaces were gained through practices. Rehabilitation is another area where robot-assisted systems are used widely. With exoskeletons and end-effectors, robot-assisted rehabilitation systems have been developed to provide precise, quantitative, and scientific rehabilitation training to the disabled [16]–[18]. By using these assistant-robots, patients can receive 1) pre-defined mandatory training exercise, 2) active support when patients have the will but find it difficult to move, and 3) rehabilitation data analysis and feedback from robots [19]. In industry, robot-assisted systems have also been developed for small-batch manufacturing and applied in arc welding, spot welding, and kitting [4], [20], [21]. By taking advantage of

Manuscript received May 24, 2019; revised September 16, 2019; accepted September 30, 2019. Date of publication November 11, 2019; date of current version April 7, 2020. This article was recommended for publication by Associate Editor M. Dotoli and Editor K. Saitou upon evaluation of the reviewers' comments. (*Corresponding author: YuMing Zhang.*)

Q. Wang, W. Jiao, R. Yu, and Y. Zhang are with the Institute for Sustainable Manufacturing, University of Kentucky, Lexington, KY 40506 USA, and also with the Department of Electrical and Computer Engineering, University of Kentucky, Lexington, KY 40506 USA (e-mail: qiyue.wang@uky.edu; wenhua.jiao@uky.edu; rui.yu@uky.edu; yuming.zhang@uky.edu).

M. T. Johnson is with the Department of Electrical and Computer Engineering, University of Kentucky, Lexington, KY 40506 USA (e-mail: mike.johnson@uky.edu).

Color versions of one or more of the figures in this article are available online at <http://ieeexplore.ieee.org>.

Digital Object Identifier 10.1109/TASE.2019.2945607

1545-5955 © 2019 IEEE. Personal use is permitted, but republication/redistribution requires IEEE permission.
See <https://www.ieee.org/publications/rights/index.html> for more information.

assistance from robots, the required skill level from human operators is greatly decreased, such that a novice operator may have the ability to finish relatively complex manufacturing tasks with a good performance.

In previous robot-assisted welding systems [4], [20], the robot reduced sharp movements of welding torch through an added impedance. A human and a robot worked together on-site, and the human was still subject to hazardous agents. There are other human–robot welding systems [22], [23] that allow a human to control the robot remotely. However, the robots only act as puppets with no intelligence, i.e., just copying the trajectory of human commands, even if the human makes mistakes. An ideal robot-assisted welding system should possess at least the following two characteristics: 1) remote operation to protect humans from dangerous welding environment and 2) intelligence to help correct human operation faults, especially from novice welders.

Understanding and recognizing human intention is the foundation to correct possible operation errors from the commanding human to effectively operate robots to perform for the human [24]. Linear dynamic models, including state models and Kalman filtering, have been proposed to model human intention and been applied to power-assisted rehabilitation robots [25], [26]. In order to characterize the nonlinearity in human intention/action, nonlinear models, including neural networks (NNs) and support vector machines (SVMs), have also been proposed to recognize the human intention for applications, such as limb trajectory tracking for robots [27], [28]. However, such deterministic models, linear or nonlinear, cannot characterize the innate randomness of human actions. To cope with this issue, some researchers have proposed to use hidden Markov models (HMMs) [29]–[34] or layered HMMs (LHMMs) [35]–[37], which contain multiple levels of HMM [38] to recognize the human intention. Two kinds of ideas have been proposed as follows.

- 1) When the human intention is defined as a task, each task is characterized as an HMM. Then, the human intention recognition (IR) problem is equivalent to the probability computation of certain sequences with the appropriate HMM [29], [30].
- 2) When the human intention is defined as a subtask, it is usually taken as the hidden state, and an entire human action sequence is modeled as an HMM. Then, the human IR problem can be stated as the hidden state estimation [32]–[34]. Both of these problems can be solved using the forward-backward algorithm [39].

To meet the requirement on the characteristics of an ideal robot-assisted welding system as analyzed above, i.e., both remote control and intelligence, we propose a virtual reality (VR) robot-assisted welding system based on human IR. This system applies customer-grade VR hardware as the interface between humans and robots. With information communicating bi-directionally via the VR system, robots can assist humans remotely. The need for on-site operation is eliminated, and the operation safety is improved. The proposed human IR component has not only some similarities to previous work but also some new aspects. In our application, human intention is defined as the intended human hand motion. In an ideal

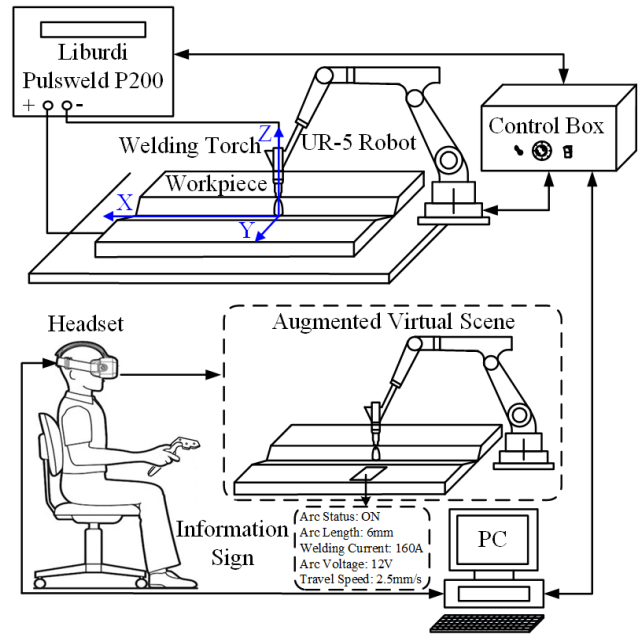


Fig. 1. Schema of VR robot-assisted welding system.

manual welding process, welding torch moves in accordance with the human intended movement. Due to the natural and inevitable vibrations of human hands, it is hard or even impossible at all for a human to control the welding torch as intended, especially for novice welders. Human hand stability training is typically an important part of welder training. We use the HMM-based concept of state occupancy probability to model instable randomness and apply an HMM-based method to recognize the human intention, using human hand movement speed as observable variables. For our proposed method, the welding tasks cannot be decomposed of subtasks in advance. Thus, the hidden state number cannot be pre-identified. To address this problem, we propose to use the Bayesian information criterion (BIC) to identify the number of hidden states in the HMMs. Training the HMM using the Baum-Welch algorithm, the hidden state occupancy probability distribution is then estimated using the forward algorithm. The robot executes intended actions determined from the statistical expectation of observable variables. Experiments show that with assistance from robots by recognizing human intention, humans can finish welding tasks with better performances. This verifies the effectiveness of the proposed VR robot-assisted welding system.

In Section II, the details of system configuration, cyber-physical model, and specialties of developed VR robot-assisted welding systems are presented. Section III discusses the principles of HMMs, followed by the details of HMM training in Section IV. Section V presents the proposed human IR algorithm. Robot-assisted welding experiments are conducted in Section VI, and conclusions are summarized in Section VII.

II. SYSTEM CONFIGURATION

A. Hardware

The schematic diagram and configuration of the developed VR robot-assisted welding system are shown in Figs. 1 and 2,

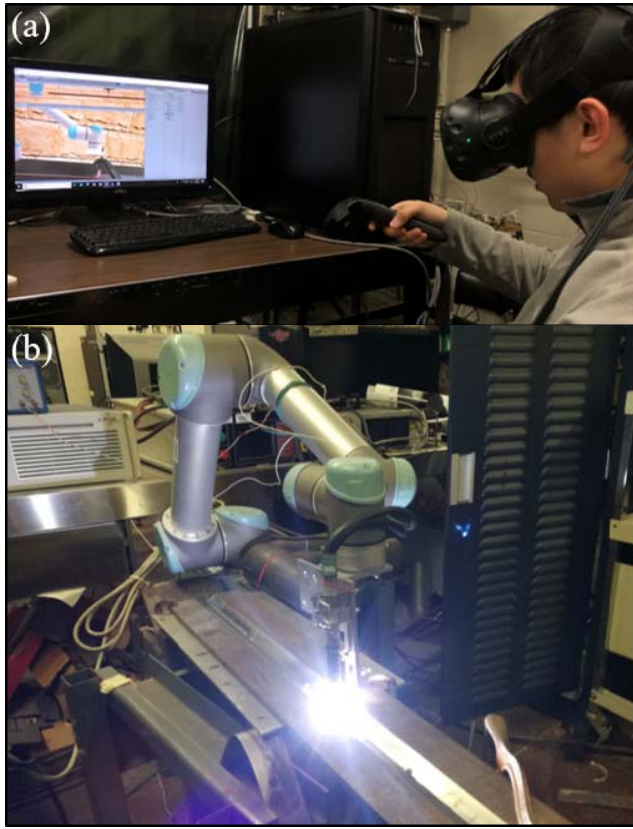


Fig. 2. Configuration of VR robot-assisted welding system. (a) Human is undertaking to weld remotely and virtually. (b) Robot is assisting human undertaking welding tasks on site.

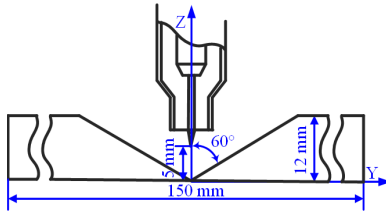


Fig. 3. Cross-section dimension of workpieces and the initial position of the welding torch.

respectively. In this system, human hand movement data is collected via the motion-tracked handle, which is a part of the customer-grade VR system, HTC Vive. This commercial VR system can track handles and the headset with submillimeter accuracy in room-scale space in real-time (with 90 Hz refresh rate) by capturing multi-markers on their surfaces and using embedded inertial measurement units (IMUs). By using motion-tracked headsets, the 3-D augmented virtual scene is shown to the operator via a head-mounted display (HMD). The gas tungsten arc welding (GTAW) torch is installed on a 6-DoF collaborative industrial robot, UR-5, and is powered by a welding power supply, Liburdi Pulsweld P200. V-groove workpieces whose cross section dimension is shown in Fig. 3 are welded with direct current electrode negative (DCEN).

B. Layered Cyber-Physical Model

The cyber-physical model of the proposed robot-assisted welding system is shown in Fig. 4. Four spaces, including user

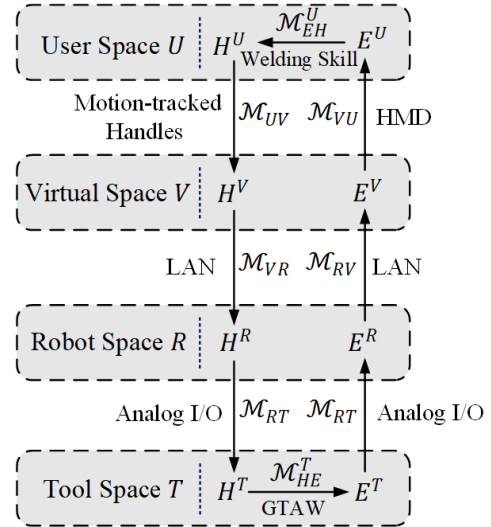


Fig. 4. Layered cyber-physical model of developed VR robot-assisted welding system: U, V, R, T are four spaces; \mathcal{M} is mapping function in the same or adjacent space(s).

space U , virtual space V , robot space R , and tool space T , coexist with the layered architecture. Via virtual space V and robot space R , the objects in user space U and tool space T map to each other. In one working cycle, the human operator observes the augmented virtual scene E^U from the headset and takes actions H^U correspondingly based on her/his welding skill modeled as \mathcal{M}_{EH}^U . Then H^U is mapped to virtual space as H^V via motion-tracked handles. H^V includes the requested welding current and welding torch movement. In robot space, the robot moves in accordance with the intended movement recognized from H^V to assist the human operator. In addition to the movement of six independent joints, the robot action H^R also includes requesting the welding current for the welding power supply. In tool space, the actions of the welding torch H^T are its movement attached to the robot and the application of the requested welding current from the welding power supply. A physical process, GTAW modeled as \mathcal{M}_{HE}^T maintains and maps welding torch behaviors to welding feedback information E^T (arc voltage and current), which is transmitted to the robot space. Robot information E^R includes robot pose and information transmitted from tool space. In virtual space, all information is integrated to render a 3-D augmented virtual environment E^V . E^V includes welding robot pose and some augmented information, including arc status, welding current, welding voltage, arc length, and travel speed. Via headset, the human observes the augmented virtual scene E^U , which is a 2-D projection of the E^V based on the position and orientation of the headset.

The interface between the user space and the virtual space is the VR system, where information flows by motion-tracked handles and the headset. Virtual space and robot are connected by the local area network (LAN) using TCP/IP protocol. Robot space and tool space are connected via analog I/O. The entire system is developed in Unity, a popular game engine

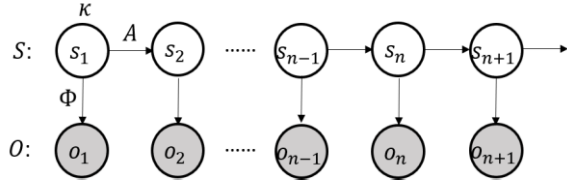


Fig. 5. Schema for HMM.

supporting almost all mainstream commercial VR systems, which is programmed with C# language.

C. System Specialties

The system has three unique characteristics designed to complete welding tasks using robotic assistance.

- 1) **Spatial separability:** by using the VR system as an interface, a human can work with the robot remotely. This spatial separability can protect the operators from onsite dangers, such as high pressure, high temperature, fumes, and radiations associated with the welding processes and environments.
- 2) **Immersive ability:** the human operators are immersed in the 3-D virtual environment generated from the information sensed from the working site. This avoids information missing due to spatial separability.
- 3) **Operative ability:** only the pose of welding torch matters for the welding process, and this can be fully accomplished by the 6-DoF robot. Moreover, by using the handles whose weight is much smaller than real welding torches, the human operators can undertake welding tasks easily, intuitively, and naturally.

III. PRINCIPLES OF HMMs

HMMs are statistical models for sequential data, where the latent state sequence is a Markov chain whose value determines the distribution of the corresponding observable variables. As shown in Fig. 5, $Z = \{z_1, z_2, z_3, \dots, z_M\}$ is the set containing all possible state values z_i , and M is the total number of possible hidden states. The instantaneous latent state s transits among Z with some probability characterized as the state transition matrix $A_{M \times M}$ where $A_{ij} \equiv P(s_n = z_j | s_{n-1} = z_i)$. With each state, the observation variable o has an emission probability distribution $P(o|z_i)$ characterized as Φ . The initial state probability vector $\kappa = [\kappa_1, \kappa_2, \dots, \kappa_M]^T$, where $\kappa_i = P(s_1 = z_i)$, is HMM's initial state distribution. Then, an HMM is determined by the three-parameter set $\theta = \{\kappa, A, \Phi\}$ completely. In our HMM, human hand movement speed $v = [v_x, v_y, v_z]^T$ is observable variable and Φ is assumed to be Gaussian distribution

$$P(o|z_i) = \frac{1}{2\pi|\Sigma_i|} \exp\left(-\frac{1}{2}(o - \mu_i)^T \Sigma_i^{-1} (o - \mu_i)\right) \quad (1)$$

where μ_i is the mean value of the speed, and Σ_i is a covariance matrix. With expanding time domain, both latent state sequence S and observable variable sequence O are formed.

IV. MODEL IDENTIFICATION

A. Principles of Baum-Welch Algorithm

As discussed previously, only the observation o is observable in our application while the latent state is unobservable. The Baum-Welch algorithm is applied to estimate the parameters of HMMs by finding the model parameters set θ maximizing the sum of the log of the likelihood function of all the observance sequences [40]

$$\hat{\theta} = \arg \max_{\theta} \left(\sum_O \log(O|\theta) \right) \quad (2)$$

where O is a single sequence. Then the parameters can be identified by finishing the iterative expectation step (E step) and maximization step (M step) in two steps:

- (1) E step: Find the Q function

$$Q(\theta, \theta^{\text{old}}) = \sum_O \sum_S (P(S|O, \theta^{\text{old}}) \log(P(O, S|\theta))). \quad (3)$$

From the properties of HMMs, $P(O, S|\theta)$ can be computed

$$P(O, S|\theta) = P(s_1|\kappa) \left(\prod_{n=2}^{N_T} P(s_n|s_{n-1}, A) \right) \prod_{n=1}^{N_T} P(o_n|s_n, \Phi) \quad (4)$$

where N_T is the length of state sequence S and observable variable sequence O .

After substituting (4) into (3), Q is separated into three parts: initial part Q_I , transition part Q_T , and emission part Q_E

$$Q(\theta, \theta^{\text{old}}) = \sum_O (Q_I + Q_T + Q_E) \quad (5)$$

$$Q_I = \sum_{i=1}^M (\gamma(s_1^i) \log(\pi_i)) \quad (6)$$

$$Q_T = \sum_{n=2}^{N_T} \sum_{i=1}^M \sum_{j=1}^M (\xi(s_{n-1}^i, s_n^j) \log(A_{ij})) \quad (7)$$

$$Q_E = \sum_{n=1}^{N_T} \sum_{i=1}^M (\gamma(s_n^i) \log(P(o_n|\Phi_i))) \quad (8)$$

where

$$\gamma(s_n^i) = P(s_n = z_i | O, \theta^{\text{old}}) \quad (9)$$

$$\xi(s_{n-1}^i, s_n^j) = P(s_{n-1} = z_i, s_n = z_j | O, \theta^{\text{old}}). \quad (10)$$

M step: Maximize the $Q(\theta, \theta^{\text{old}})$ with respect to θ :

Since Q is a continuous function of θ , its value is maximized when the partial derivative of Q with respect to θ is 0

$$\frac{\partial Q(\theta, \theta^{\text{old}})}{\partial \theta} = 0 \Leftrightarrow \begin{cases} \frac{\partial Q(\theta, \theta^{\text{old}})}{\partial \kappa_i} = 0 \\ \frac{\partial Q(\theta, \theta^{\text{old}})}{\partial A_{ij}} = 0 \\ \frac{\partial Q(\theta, \theta^{\text{old}})}{\partial \mu_i} = 0 \\ \frac{\partial Q(\theta, \theta^{\text{old}})}{\partial \Sigma_i} = 0. \end{cases} \quad (11)$$

The iterative learning algorithm for the HMMs can be given as

$$\theta = \begin{cases} \kappa_i = \frac{\sum_O \gamma(s_i^i)}{\sum_O \sum_{i=1}^M \gamma(s_i^i)} \\ A_{ij} = \frac{\sum_O \sum_{n=2}^{N_T} (\xi(s_{n-1}^i, s_n^j))}{\sum_O \sum_{k=1}^M \sum_{n=2}^{N_T} (\xi(s_{n-1}^i, s_n^k))} \\ \mu_i = \frac{\sum_O \sum_{n=1}^{N_T} (\gamma(s_n^i) \cdot o_n)}{\sum_O \sum_{n=1}^{N_T} \gamma(s_n^i)} \\ \Sigma_i = \frac{\sum_O \sum_{n=1}^{N_T} (\gamma(s_n^i) \cdot (o_n - \mu_i)(o_n - \mu_i)^T)}{\sum_T \sum_{n=1}^{N_T} \gamma(s_n^i)}. \end{cases} \quad (12)$$

Additionally, the unknown variables γ and ξ can be computed using the forward-backward algorithm:

The forward probability α_n^i and the backward probability β_n^i are defined as

$$\alpha_n^i \equiv P(o_1, o_2, \dots, o_n, s_n = z_i) \quad (13)$$

$$\beta_n^i \equiv P(o_{n+1}, o_{n+2}, \dots, o_{N_T} | s_n = z_i) \quad (14)$$

where both α_n^i and β_n^i can be computed using the dynamic programming (DP) algorithm

$$\begin{cases} \alpha_1^i = \kappa_i P(o_1 | z_i) \\ \alpha_{n+1}^i = \left(\sum_{j=1}^M (\alpha_{n+1}^j A_{ji}) \right) P(o_{n+1} | z_i) \end{cases} \quad (15)$$

$$\begin{cases} \beta_{N_T}^i = 1 \\ \beta_{n-1}^i = \sum_{j=1}^M (A_{ij} \beta_n^j P(o_n | z_j)). \end{cases} \quad (16)$$

Following this, both γ and ξ can be computed explicitly:

$$\begin{aligned} \gamma(s_n^i) &= P(s_n = z_i | O, \theta^{\text{old}}) \\ &= \frac{P(s_n = z_i, O | \theta^{\text{old}})}{P(O | \theta^{\text{old}})} = \frac{\alpha_n^i \beta_n^i}{\sum_{i=1}^M \alpha_n^i \beta_n^i} \end{aligned} \quad (17)$$

$$\begin{aligned} \xi(s_{n-1}^i, s_n^j) &= P(s_{n-1} = z_i, s_n = z_j | O, \theta^{\text{old}}) \\ &= \frac{P(s_{n-1} = z_i, s_n = z_j, O | \theta^{\text{old}})}{P(O | \theta^{\text{old}})} \\ &= \frac{\alpha_{n-1}^i A_{ij} P(o_n | z_i) \beta_n^j}{\sum_{i=1}^M \alpha_{n-1}^i \beta_n^j}. \end{aligned} \quad (18)$$

Together, these algorithms allowing estimation of all the variables needed to identify the parameters of the HMMs have been derived explicitly.

B. Data Collection

The experimental task consists of a user (one of the authors) using motion-tracked handles to implement a pulse backing welding task eight separate times, generating eight training sequences. The applied welding parameters are shown in Table I. The position of the human hand is sensed with a sampling frequency of 10 Hz. Hand speed is determined based on the position data. In total, eight observable variable sequences with 6585 data points are used to train models.

TABLE I
WELDING PARAMETERS APPLIED

Welding Parameters	Value
Peak Current (A)	160
Base Current (A)	40
Pulse Frequency (Hz)	1
Duty Cycle	50%
Initial Arc Length (mm)	5
Tungsten Diameter (mm)	2.4
Tungsten Grind Angle (°)	30
Shielded Gas	Argon
Gas Flow (SCCM)	4700
Workpiece Material	DH36

C. Identification of Hidden State Number

As discussed in Section I, unlike previous methods for modeling human actions using HMMs, the number of hidden states cannot be identified in advance. Therefore, the BIC is used to identify the best number of hidden states. For HMMs, the BIC can be computed as

$$BIC = -2 \cdot \log(L) + k \cdot \log(n) \quad (19)$$

where the L is the maximized value of the likelihood of observable data with the model

$$L = \max_{\theta} \left(\prod_O P(O | \theta) \right) = \max_{\theta} \left(\prod_O \left(\sum_{i=1}^M \alpha_{N_T}^i \right) \right) \quad (20)$$

k is the number of independent parameters learned in HMMs, and n is the total number of data points, 6585 in our application.

For our application, the emission probability is assumed to have a Gaussian distribution and k is the sum of the learned number of the four independent parameters

$$k = k_{\kappa} + k_A + k_{\mu} + k_{\Sigma} \quad (21)$$

$$k_{\kappa} = M - 1 \quad (22)$$

$$k_A = M \cdot (M - 1) \quad (23)$$

$$k_{\mu} = d \cdot M \quad (24)$$

$$k_{\Sigma} = d \cdot (d + 1) \cdot M / 2 \quad (25)$$

where M is the number of hidden states, and d is the data feature dimension. In our application, $o = v = [v_x, v_y, v_z]^T$ which is the hand movement speed, and therefore, $d = 3$. Thus

$$k = M^2 + 9M - 1. \quad (26)$$

Using the algorithm presented in part A, the HMMs are trained with fully random initial model parameters. In order to decrease the effect of randomly choosing initial model parameters, models with the same number of hidden states are trained ten times. Finally, the number of hidden states is identified as 5 by computing and comparing scores and BIC for each model. These results are shown in Fig. 6. The score of each model is defined as the log of the likelihood of observable data

$$\text{score} = \log \left(\prod_O P(O | \theta) \right) = \sum_O \left(\log \left(\sum_{i=1}^M \alpha_{N_T}^i \right) \right). \quad (27)$$

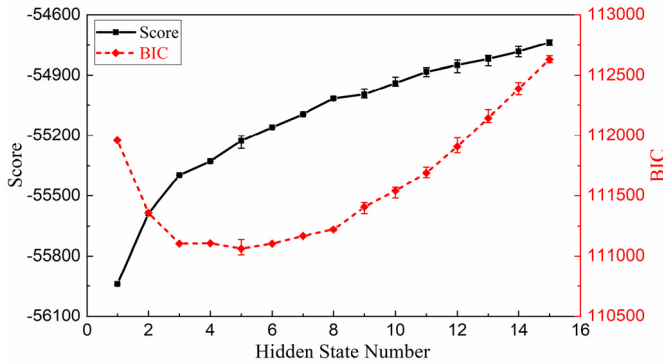


Fig. 6. Model evaluation with different number of states.

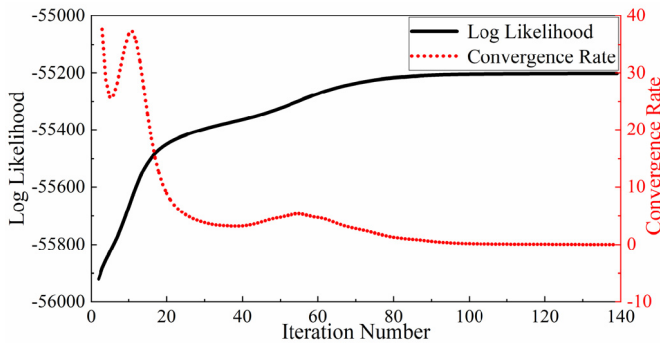


Fig. 7. Convergence in model training.

D. Model Training

By taking the number of hidden states as 5, the HMM training is repeated ten times with initial parameters chosen randomly. The one with the highest score is chosen as the final model. The iterative process is shown in Fig. 7. The convergence rate is defined as the difference of the log-likelihood of observable sequences compared with the last iteration. It can be found that the model converges after ~ 100 iterations.

V. HUMAN INTENTION RECOGNITION

A. Principles

Unintentional actions exist in the operation/demonstration of commanding humans because of physical limitation that reduces the controllability and the lack of the needed degree of skills. The robot should, thus, execute the intended operations recognized. The waveform of the welding current is not easy to adjust in real-time by a human as the tool/torch. Hence, in our case, the former is pre-determined and fixed, and the latter is real-time adjusted as in manually operated welding process.

We define human intention as the intended hand speed \bar{v} . The problem can, thus, be stated as that of estimating the current/present intended movement speed \bar{v}_n from the raw moving speed sequence. This problem can be addressed in two steps.

1) *State Occupancy Probability Computation*: The state occupancy probability vector ζ_n characterizes the probability

TABLE II
STATISTICAL INFORMATION FOR TESTING EXPERIMENTS

Speed		Statistical Information (mm/s)	
		Mean	Standard Deviation
X	Raw	2.53	5.03
	Intended	2.54	1.51
Y	Raw	0.022	3.17
	Intended	-0.001	0.92
Z	Raw	0.061	5.08
	Intended	0.010	0.30

of occurrence of each hidden state z_i at a given time

$$\zeta_n = [\zeta_n^1, \zeta_n^1, \dots, \zeta_n^M]^T \quad (28)$$

$$\zeta_n^i \equiv P(s_n = z_i | o_1, o_2, \dots, o_n). \quad (29)$$

Here, each hidden state z_i is considered as a “base state” and the state at any time s_n is estimated as the probability-weighted mixture of base state z_i . The probability vector ζ_n can be computed based on the forward algorithm

$$\zeta_n^i = \frac{P(s_n = z_i, o_1, o_2, \dots, o_n)}{P(o_1, o_2, \dots, o_n)} = \frac{\alpha_n^i}{\sum_{i=1}^M \alpha_n^i}. \quad (30)$$

2) *Intended Movement Estimation*: For each hidden state z_i , the u_i is considered as its intended movement. The intended movement at each time is estimated as the statistical expectation of current observable variable based on state occupancy probability vector ζ_n

$$\bar{v}_n = \sum_{i=1}^M (\zeta_n^i \cdot \mu_i). \quad (31)$$

B. Testing Verification

Another movement sequence is generated by the same person with the same experimental configuration to test the effectiveness of the proposed human intention algorithm. The recognized intended speed results and its statistical information are shown in Fig. 8 and Table II. From Fig. 8 and Table II, it can be found that the intended movement estimated using the HMM approach is much smoother, with significantly lower standard deviation and near-zero means in the y- and z-directions. Smoother movement is more preferred for welding: with consistent motion in the direction of travel and little or no motion in the lateral and vertical directions. As can be seen, in the primary direction of travel along the x-axis, the recognized intended travel speed achieves a mean close to the true one and a decreased standard deviation. In the lateral y-axis and vertical z-axis direction, a near-zero mean and decreased standard deviation are also achieved.

An interesting phenomenon happens in the z-direction. The raw speed data has the largest variance, but the intended speed data has the smallest variance. This indicates that the z-direction movement has the highest degree of randomness, i.e., there is no obvious intention transition for humans in the z-direction movement compared with the other two directions.

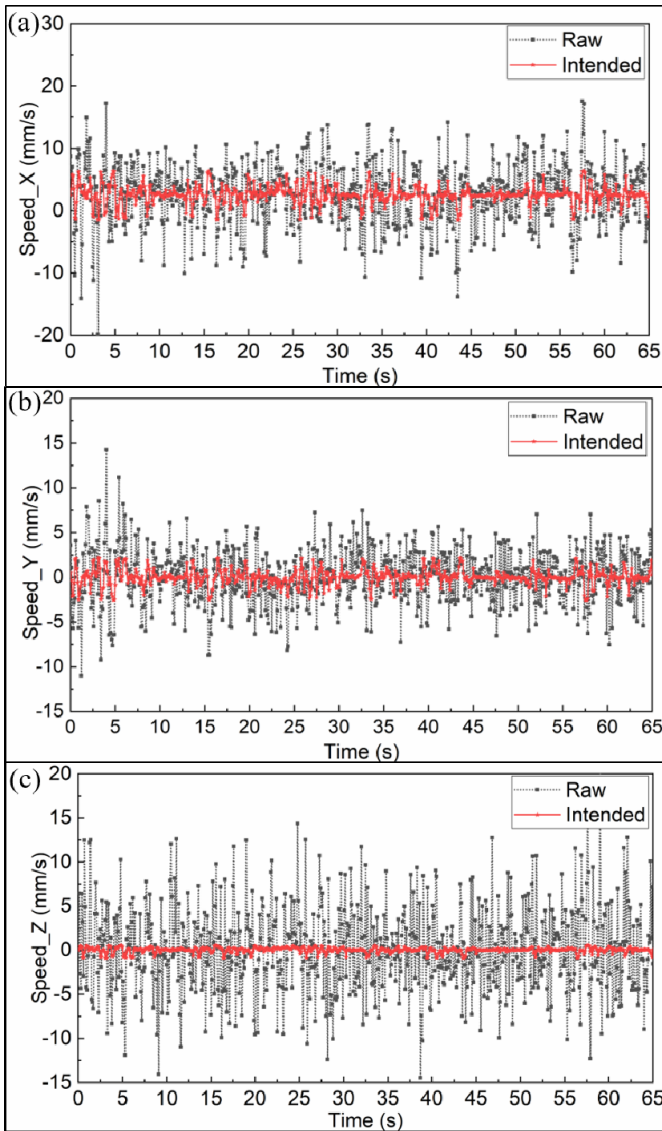


Fig. 8. Human IR result (a) x -direction in which the welding torch moves along, (b) y -direction where welding torch deviates from weld seam, and (c) vertical z -direction.

That makes sense since the x -direction is the primary welding direction, for which the human operator has a clear intended travel speed, and the y -direction is the weld seam position where the operator intends to track. The z -direction is the vertical direction where there is no strict regulation for the operator as long as the continuity of the welding process is maintained. Furthermore, the vertical movement is much harder to control than horizontal movement for humans due to internal muscle structure.

VI. ROBOT-ASSISTED WELDING EXPERIMENT

The trajectories of the robot with and without using the proposed human IR algorithm are shown in Fig. 9. The corresponding welded workpieces using the same welding parameters in Table I are shown in Fig. 10. Based on the human operator movement and weld bead appearance, the welding

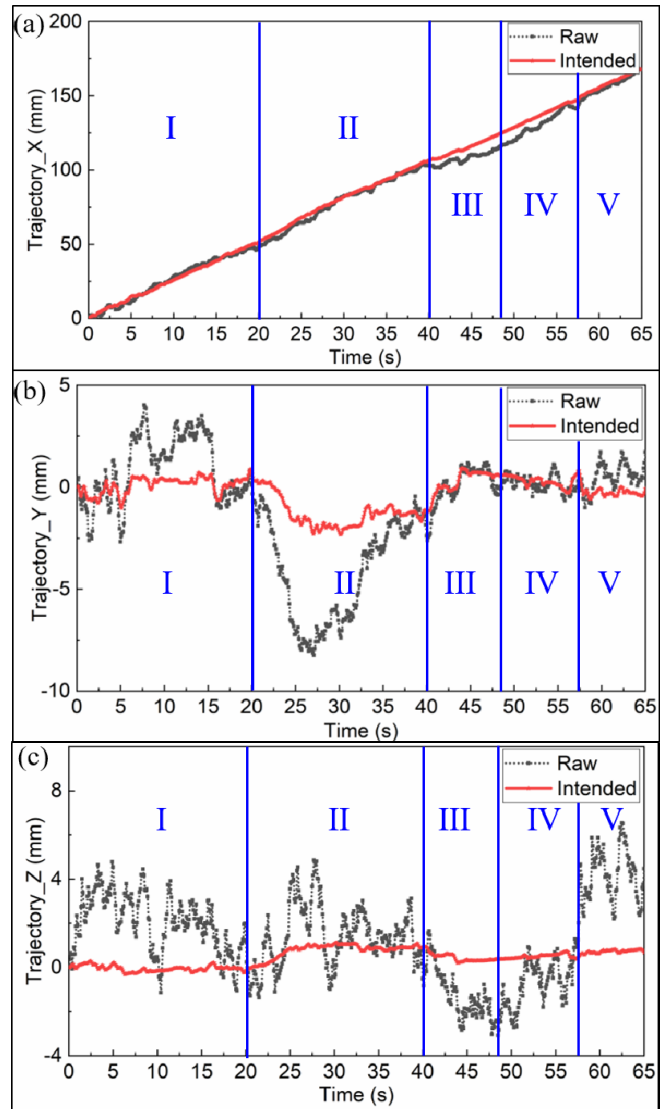


Fig. 9. Robot trajectory (a) x -direction, (b) y -direction, and (c) z -direction.

operation can be separated into five stages: I (0–20 s); II (20–40 s); III (40–48 s); IV (48–57.5 s) and V (57.5–65 s).

In stage I, the welding process is relatively steady; there is no big difference between the raw movement and the intended movement such that the corresponding weld bead appearances are similar. In stage II, the position of the tungsten electrode deviates from and returns to the weld seam, with a maximum seam deviation of ~ 8 mm. This causes the heat from the arc to the workpiece to deviate from the weld seam. This deviation results in a critical welding failure (incomplete weld). The seam deviation comes from the accumulation of the negative speed in the lateral y -axis at 21–27 s. This can be considered as an unintended operation fault by the operator. When the operator realizes this problem via the HMD, he/she tries to correct by adjusting the position of the welding torch to track the weld seam again (27–40 s). When using the intended operation recognized from the proposed HMM-based human IR algorithm, the sharp change of operation speed in the y -axis during stage II is suppressed. The maximum seam deviation

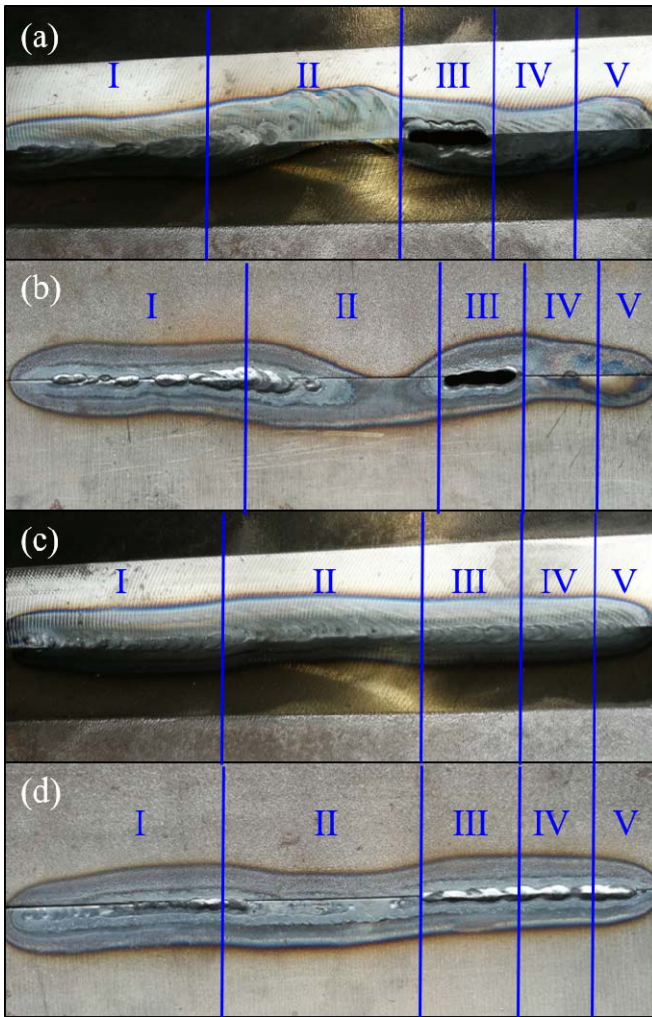


Fig. 10. Welded workpieces (a) front side without human IR, (b) backside without human IR, (c) front side with human IR, and (d) backside with human IR.

is reduced to ~ 2.5 mm, which still results in the incomplete penetration defect, but the degree of harm has been decreased, and the incomplete penetration is often acceptable except for critical cases.

In stage III, the travel speed along the x-axis is too low, resulting in high total energy input and eventual burn-through welding failure. The opposite problem occurs in stage IV, with high travel speed resulting in low total energy input and incomplete penetration. Using the proposed algorithm, the variance in travel speed is much lower, and both the stage III low-speed and stage IV high-speed welding faults are eliminated.

In stage V, the trajectory of the tungsten electrode along the vertical z-axis vibrates above the desired center position resulting in a longer arc than desired, with a maximum arc length of ~ 12 mm compared with an initial arc length of 5 mm. As shown in Fig. 11, this causes a strong divergence of the arc in the workpiece. The arc heat to workpiece spreads so much that the energy density is insufficient for full fusion of base metal, causing an incomplete penetration defect. After using the proposed algorithm, the variation above the desired

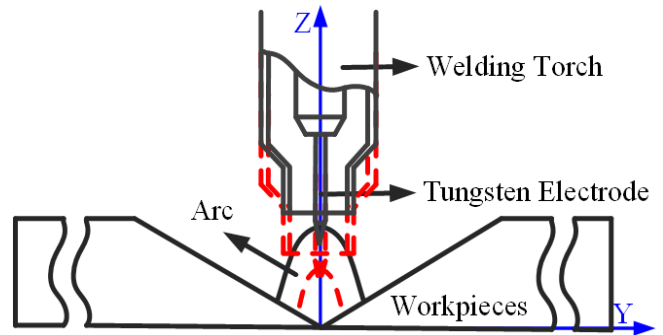


Fig. 11. Schema of arc shape with the vertical movement of the welding torch. Red dash: original shape. Black solid: arc diverges with arc lengthening.

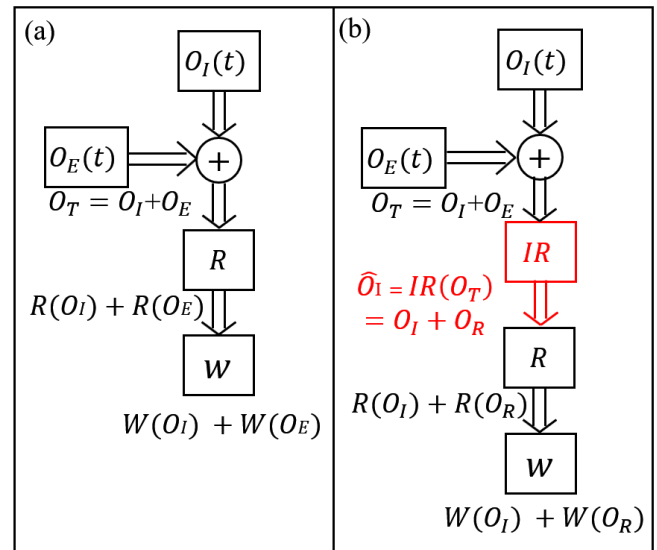


Fig. 12. Principle of robot-assisted manual welding (a) without human IR and (b) with human IR.

z-axis position is suppressed, and the maximum arc length is maintained at ~ 6 mm and not creating a welding fault.

Fig. 12 illustrates how the human IR helps improve the performance. The raw human operation O_T includes the intended operation O_I and erroneous one O_E . Without the IR, the robot (modeled as R) manipulates the movement of the welding torch by copying O_T . Both O_I and O_E affect the welding (modeled as R) to produce $W(O_I)$ and $W(O_E)$, where the former is desired, but the latter is not. After adding the human IR component IR , as shown in Fig. 12(b), the recognized intended operation \hat{O}_I contains O_I and residual part O_R

$$\hat{O}_I = O_I + O_R. \quad (32)$$

Via the same robot and welding system as modeled by R and W , the final welding results are now controlled by O_I and O_R . The goal of this article for human IR is to minimize O_R such that $O_R \ll O_E$. In our welding experiments without human IR, the generated weld faults (such as incomplete weld and burn-through) can be considered as $W(O_E)$ due to erroneous human operations. After using the proposed human IR algorithm, the remaining weld defects (such as incomplete penetration) are due to O_R . For an effective human

IR algorithm such that $O_R \ll O_E$, $W(O_R)$ must be much smaller than $W(O_E)$ as R and W are unchanged.

VII. CONCLUSION

This article has introduced a CPS with a layered architecture, which allows robots to assist human operators in performing welding and improve performance. For protecting operators from onsite dangers, a VR environment has been created using customer-grade VR hardware as the operating interface to separate humans and robots spatially. A human IR algorithm is developed based on HMMs using hand velocity as observable variables. The number of hidden states is identified using BIC, and the HMM is trained using the Baum-Welch algorithm. Intended movement is estimated using state estimation and expected observable variable estimation. A welding experiment based on this method has been implemented. The results indicate that human welding operators have substantially better performance when using the proposed VR robot-assisted welding system.

REFERENCES

- [1] J. Sprovieri. (2016). *New Technology for Robotic Welding*. [Online]. Available: <https://www.assemblymag.com/articles/93555-new-technology-for-robotic-welding>
- [2] O. Popović, R. Prokić-Cvetković, M. Burzić, U. Lukić, and B. Beljić, "Fume and gas emission during arc welding: Hazards and recommendation," *Renew. Sustain. Energy Rev.*, vol. 37, pp. 509–516, Sep. 2014.
- [3] J. Dallos. (2017). *Combating the Welder Shortage*. [Online]. Available: <https://www.fabtechexpo.com/blog/2017/12/04/combating-the-welder-shortage>
- [4] M. S. Erden and A. Billard, "Robotic assistance by impedance compensation for hand movements while manual welding," *IEEE Trans. Cybern.*, vol. 46, no. 11, pp. 2459–2472, Nov. 2016.
- [5] N. Enayati, E. De Momi, and G. Ferrigno, "Haptics in robot-assisted surgery: Challenges and benefits," *IEEE Rev. Biomed. Eng.*, vol. 9, pp. 49–65, 2016.
- [6] J. Konstantinova, A. Jiang, K. Althoefer, P. Dasgupta, and T. Nanayakkara, "Implementation of tactile sensing for palpation in robot-assisted minimally invasive surgery: A review," *IEEE Sensors J.*, vol. 14, no. 8, pp. 2490–2501, Aug. 2014.
- [7] J. Marescaux *et al.*, "Transatlantic robot-assisted telesurgery," *Nature*, vol. 413, no. 6854, pp. 379–380, 2001.
- [8] S. McKinley *et al.*, "A single-use haptic palpation probe for locating subcutaneous blood vessels in robot-assisted minimally invasive surgery," in *Proc. IEEE Int. Conf. Automat. Sci. Eng. (CASE)*, Aug. 2015, pp. 1151–1158.
- [9] A. R. Lanfranco, A. E. Castellanos, J. P. Desai, and W. C. Meyers, "Robotic surgery: A current perspective," *Ann. Surg.*, vol. 239, pp. 14–21, Jan. 2004.
- [10] G. T. Sung and I. S. Gill, "Robotic laparoscopic surgery: A comparison of the da Vinci and Zeus systems," *Urology*, vol. 58, no. 6, pp. 893–898, 2001.
- [11] L. Morelli, S. Guadagni, G. Di Franco, M. Palmeri, G. Di Candio, and F. Mosca, "Da Vinci single site surgical platform in clinical practice: A systematic review," *Int. J. Med. Robot. Comput. Assist. Surg.*, vol. 12, no. 4, pp. 724–734, Dec. 2016.
- [12] E. M. Suero *et al.*, "Improving the human-robot interface for telemanipulated robotic long bone fracture reduction: Joystick device vs. haptic manipulator," *Int. J. Med. Robot. Comput. Assist. Surg.*, vol. 14, no. 1, pp. 1863–1870, Feb. 2018.
- [13] L. Meli, C. Pacchierotti, and D. Prattichizzo, "Sensory subtraction in robot-assisted surgery: Fingertip skin deformation feedback to ensure safety and improve transparency in bimanual haptic interaction," *IEEE Trans. Biomed. Eng.*, vol. 61, no. 4, pp. 1318–1327, Apr. 2014.
- [14] C. Schneider, C. Ngan, R. Rohling, and S. Salcudean, "Tracked "pick-up" ultrasound for robot-assisted minimally invasive surgery," *IEEE Trans. Biomed. Eng.*, vol. 63, no. 2, pp. 260–268, Feb. 2016.
- [15] S. Basov *et al.*, "Robot-assisted laser tissue soldering system," *Biomed. Opt. Express*, vol. 9, no. 11, pp. 5635–5644, 2018.
- [16] F. J. Badesa, R. Morales, N. Garcia-Aracil, J. M. Sabater, C. Perez-Vidal, and E. Fernandez, "Multimodal interfaces to improve therapeutic outcomes in robot-assisted rehabilitation," *IEEE Trans. Syst., Man, Cybern. C, Appl. Rev.*, vol. 42, no. 6, pp. 1152–1158, Nov. 2012.
- [17] H. I. Krebs *et al.*, "Robot-aided neurorehabilitation: A robot for wrist rehabilitation," *IEEE Trans. Neural Syst. Rehabil. Eng.*, vol. 15, no. 3, pp. 327–335, Sep. 2007.
- [18] W. H. Chang and Y.-H. Kim, "Robot-assisted therapy in stroke rehabilitation," *J. Stroke*, vol. 15, no. 3, pp. 174–181, Sep. 2013.
- [19] W. Meng, Q. Liu, Z. D. Zhou, Q. S. Ai, B. Sheng, and S. Q. Xie, "Recent development of mechanisms and control strategies for robot-assisted lower limb rehabilitation," *Mechatronics*, vol. 31, pp. 132–145, Oct. 2015.
- [20] M. S. Erden and B. Marić, "Assisting manual welding with robot," *Robot. Comput.-Integr. Manuf.*, vol. 27, no. 4, pp. 818–828, 2011.
- [21] K. R. Guerin, C. Lea, C. Paxton, and G. D. Hager, "A framework for end-user instruction of a robot assistant for manufacturing," in *Proc. IEEE Int. Conf. Robot. Automat. (ICRA)*, May 2015, pp. 6167–6174.
- [22] S. J. Chen, N. Huang, Y. K. Liu, and Y. M. Zhang, "Machine assisted manual torch operation: System design, response modeling, and speed control," *J. Intell. Manuf.*, vol. 28, no. 6, pp. 1249–1258, Aug. 2017.
- [23] Y. Liu and Y. Zhang, "Toward welding robot with human knowledge: A remotely-controlled approach," *IEEE Trans. Autom. Sci. Eng.*, vol. 12, no. 2, pp. 769–774, Apr. 2015.
- [24] A. Kleinsmith and N. Bianchi-Berthouze, "Affective body expression perception and recognition: A survey," *IEEE Trans. Affect. Comput.*, vol. 4, no. 1, pp. 15–33, Jan. 2013.
- [25] J. Huang, W. Huo, W. Xu, S. Mohammed, and Y. Amirat, "Control of upper-limb power-assist exoskeleton using a human-robot interface based on motion intention recognition," *IEEE Trans. Autom. Sci. Eng.*, vol. 12, no. 4, pp. 1257–1270, Oct. 2015.
- [26] K. Wakita, J. Huang, P. Di, K. Sekiyama, and T. Fukuda, "Human-walking-intention-based motion control of an omnidirectional-type cane robot," *IEEE/ASME Trans. Mechatronics*, vol. 18, no. 1, pp. 285–296, Feb. 2013.
- [27] Y. Li and S. S. Ge, "Human-robot collaboration based on motion intention estimation," *IEEE/ASME Trans. Mechatronics*, vol. 19, no. 3, pp. 1007–1014, Jun. 2014.
- [28] T. Mei, X.-S. Hua, H.-Q. Zhou, and S. Li, "Modeling and mining of users' capture intention for home videos," *IEEE Trans. Multimedia*, vol. 9, no. 1, pp. 66–77, Jan. 2010.
- [29] L. Piyathilaka and S. Kodagoda, "Human activity recognition for domestic robots," in *Field and Service Robotics*. Cham, Switzerland: Springer, 2015, pp. 395–408.
- [30] K. Khokar, R. Alqasemi, S. Sarkar, K. Reed, and R. Dubey, "A novel telerobotic method for human-in-the-loop assisted grasping based on intention recognition," in *Proc. IEEE Int. Conf. Robot. Automat. (ICRA)*, May/Jun. 2014, pp. 4762–4769.
- [31] R. Kelley, A. Tavakkoli, C. King, A. Ambardekar, M. Nicolescu, and M. Nicolescu, "Context-based Bayesian intent recognition," *IEEE Trans. Auto. Mental Develop.*, vol. 4, no. 3, pp. 215–225, Sep. 2012.
- [32] H. Berndt, J. Emmert, and K. Dietmayer, "Continuous driver intention recognition with hidden Markov models," in *Proc. 11th Int. IEEE Conf. Intell. Transp. Syst.*, Oct. 2008, pp. 1189–1194.
- [33] N. Stefanov, A. Peer, and M. Buss, "Online intention recognition for computer-assisted teleoperation," in *Proc. IEEE Int. Conf. Robot. Autom.*, May 2010, pp. 5334–5339.
- [34] G. Saponaro, G. Salvi, and A. Bernardino, "Robot anticipation of human intentions through continuous gesture recognition," in *Proc. Int. Conf. Collaboration Technol. Syst. (CTS)*, May 2013, pp. 218–225.
- [35] D. Aarno and D. Kragic, "Layered HMM for motion intention recognition," in *Proc. IEEE/RSJ Int. Conf. Intell. Robots Syst.*, Oct. 2006, pp. 5130–5135.
- [36] D. Aarno and D. Kragic, "Motion intention recognition in robot assisted applications," *Robot. Auto. Syst.*, vol. 56, no. 8, pp. 692–705, Aug. 2008.
- [37] C. Zhu and W. Sheng, "Wearable sensor-based hand gesture and daily activity recognition for robot-assisted living," *IEEE Trans. Syst., Man, Cybern. A, Syst., Humans*, vol. 41, no. 3, pp. 569–573, May 2011.
- [38] N. Oliver, A. Garg, and E. Horvitz, "Layered representations for learning and inferring office activity from multiple sensory channels," *Comput. Vis. Image Understand.*, vol. 96, no. 2, pp. 163–180, Nov. 2004.
- [39] L. Rabiner, "A tutorial on hidden Markov models and selected applications in speech recognition," *Proc. IEEE*, vol. 77, no. 2, pp. 257–286, Feb. 1989.
- [40] C. M. Bishop, *Pattern Recognition and Machine Learning*. Cham, Switzerland: Springer, 2006.



Qiyue Wang received the B.Eng. degree in welding engineering from the Harbin Institute of Technology, Harbin, China, in 2016. He is currently pursuing the Ph.D. degree in electrical engineering with the University of Kentucky, Lexington, KY, USA.

He was a Manufacturing Intern (welding and joining) with Tesla, Inc., Fremont, CA, USA, from June to December 2018. His current research interests include human–robot interaction (HRI), machine learning, and their applications in welding robots.

Mr. Wang has published one article in the IEEE ROBOTICS AND AUTOMATION LETTERS (RA-L).



Wenhua Jiao received the B.S. degree in electrical engineering from the University of Kentucky, Lexington, KY, USA, in 2015, where he is currently pursuing the Ph.D. degree in electrical engineering.

He was an Intern (welding and joining team) with Tesla, Inc., Fremont, CA, USA, from January to May 2018. His current research interests include image processing and intelligent welding.



Rui Yu received the B.Eng. degree in information engineering from the Xi'an University of Posts & Telecommunications, Xi'an, China, in 2014, and the M.Eng. degree in electrical engineering from the University of Kentucky, Lexington, KY, USA, in 2018, where he is currently pursuing the Ph.D. degree in electrical engineering.

He worked as a Software Test Engineer with Xi'an Hanghua Information Technology Co., Ltd., Xi'an, from July 2014 to May 2015. His current research interests include machine vision, machine learning,

and their applications in welding robots.

Mr. Yu has worked as a third author in two IEEE articles.



Michael T. Johnson (SM'01) received the B.S. degrees in computer science engineering and engineering with electrical concentration from LeTourneau University, Longview, TX, USA, in 1989 and 1990, respectively, the M.S. degree in electrical engineering from The University of Texas at San Antonio, San Antonio, TX, USA, in 1994, and the Ph.D. degree from Purdue University, West Lafayette, IN, USA, in 2000.

He was a Visiting Professor with Tsinghua University, Beijing, China, from 2008 to 2009 and from 2014 to 2015. He is currently a Professor and the Chair of Electrical and Computer Engineering with the University of Kentucky, Lexington, KY, USA. His primary research area is speech and signal processing, with interests in articulatory kinematics, bioacoustics, and machine learning.



YuMing Zhang (SM'96) received the B.S. and M.S. degrees in control major and the Ph.D. degree in welding major from the Harbin Institute of Technology, Harbin, China, in 1982, 1984, and 1990, respectively.

He is currently a Professor and the James R. Boyd Professor of Electrical Engineering with the University of Kentucky, Lexington, KY, USA. He has coauthored over 190 peer-reviewed journal publications and has been granted nine U.S. patents. His research interests include welding processes sensing and control, robotic/intelligent welding, and human–robot collaborative welding.

Dr. Zhang's recognitions include a fellow of the American Welding Society (AWS), ASME, and SME. He received the William Irrgang Memorial Award (in 2017) from the AWS, the Dean's Award for Excellence in Research (in 2016) from the College of Engineering, University of Kentucky, and the Poster Paper Prize and the Application Paper Finalist (in 2002) from the 15th IFAC World Congress. He currently serves the AWS as a Lead Principal Reviewer for the *Welding Journal* and the Chair for the Technical Papers Committee.